Energy Science & Engineering

WILEY

ORIGINAL ARTICLE OPEN ACCESS

Assessment of Voltage Unbalance and Power Losses in Distribution Network Integrated With PVs and EV Charging Stations

Maaz Ahmad[1] | Aamir Nawaz[1] | Rahmat Ullah[2] | Ehtasham Mustafa[1] | Abdelfatah Ali[3,4]

[1]Department of Electrical Engineering, Gomal University, Dera Ismail Khan, Khyber Pakhtunkhwa, Pakistan | [2]Advanced High Voltage Engineering Research Centre, Cardiff University, Cardiff, UK | [3]Department of Electrical Engineering, South Valley University, Qena, Egypt | [4]Department of Electrical Engineering, American University of Sharjah, Sharjah, United Arab Emirates

Correspondence: Rahmat Ullah (ullahr1@cardiff.ac.uk)

Received: 6 April 2025 | **Revised:** 15 September 2025 | **Accepted:** 1 December 2025

Keywords: active power loss | electric vehicles charging stations | photovoltaics | unbalanced radial distribution systems | voltage unbalanced factor

ABSTRACT

Unequal load distribution in three-phase power distribution networks leads to voltage unbalance and decreased network efficiency. Integration of photovoltaics (PVs) and electric vehicle charging stations (EVCSs) into such networks is a challenging task as their penetration affects the power quality of the system. Considering the varying load demand and PV generation alongside the stochastic nature of electric vehicles (EVs), this study presents a technique for the precise placement of the PV system and EVCS inside the unbalanced networks to enhance the performance of the system. The optimal placement of PVs and EVCSs is carried out by considering real Pakistani 60-bus unbalanced radial distribution systems (URDS), whereas to minimize the voltage unbalanced factor (VUF) and active power loss (APL), a metaheuristic technique, improved grey wolf optimization (IGWO) was used. Six different case studies of the integration of PVs and EVCSs inside the system are considered in this work. The simulation results demonstrate that the integration of the single-phase PVs and EVCSs resulted in an increase of APL by 18.04% and VUF by 21.78%. However, the APL and VUF decreased by 14.82% and 3.96%, respectively, for the three-phase integration of the same size of PVs and EVCSs. Hence, the integration of three-phase PVs and EVCSs enhanced the system performance in comparison to the single-phase integration.

1 | Introduction

The developing countries are working on several initiatives to persuade consumers to switch from internal combustion engine (ICE) to electric vehicle (EV) technology and invest in renewable energy sources (RES) to keep the environment eco-friendly [1]. The distribution networks integrated with photovoltaic (PV) encounter significant challenges, including the intermittent and dynamic nature of these sources [2]. The existing distribution networks in these countries cannot meet the increasing demand for EVs. Meanwhile, the high penetration of PVs and EVCSs influences the operational performance along with power quality parameters such as power losses and VUF of the network. The abnormal increase in VUF and power losses can lead to overheating and potential damage to electrical equipment [3]. Moreover, inappropriate PV size and location may adversely influence network conditions, including power quality. Henceforth, it is essential to employ a

Abbreviations: σ, Standard deviation; APL, active power loss; BESS, battery energy storage system; DERs, distributed energy resources; DGs, distribution generations; EVCS, electric vehicle charging station; EVs, electric vehicles; HV, high voltage; ICE, internal combustion engine; IGWO, improved grey wolf optimization; LV, low voltgae; PEVs, plugin electric vehicles; PVs, photo voltaic; SOC, state of charge; URDS, unbalanced radial distribution network; VUF, voltage unbalance factor.

All authors contributed equally to this work.

suitable strategy to address the power quality and intermittent nature of PVs simultaneously to enhance the distribution network's stability, reliability, and efficiency. This research aims to mitigate the VUF and APL by the appropriate selection and location of PVs and EVCSs in an unbalanced distribution network.

Modern power distribution networks present significant challenges for utility companies, primarily due to their unbalanced nature stemming from the uneven distribution of loads across the three phases. This situation results in increased line losses, a reduction in voltage stability, and an increase in voltage unbalance at the distribution transformer [4]. The importance of PVs in electricity networks cannot be overstated, as they represent a vital energy source that connects directly to the distribution system or is located at the consumer premises. By facilitating localized energy production, PVs not only support grid stability but also empower consumers to engage more actively in energy management and sustainability efforts. However, utilizing EVs as a spinning reserve to meet peak demand and enhance system performance may optimize the location of the charging station (CS). As a result, EVs may help reduce expenses and optimize critical factors like voltage deviation and power losses across the network. However, selecting the appropriate size and location of the PVs and EVCSs in the unbalanced distribution networks is important, as they have catastrophic effects on voltage stability and power losses. In recent times, numerous studies have been carried out to address the challenges associated with PVs and EVCSs integration, where various metaheuristic approaches have been adopted.

A multi-criteria decision-making technique has been formulated by Maji et al. [5] to improve the network performance metrics of unbalanced power distribution networks (PDNs). Prior research has shown that the main goal of strategically deploying PV systems throughout the network is to mitigate active power losses. Soliman et al. [6] have devised a specific methodology for hosting PVs in the distribution system to enhance the system performance parameters and decrease the annual operating expenses. Considering the hourly and seasonal fluctuations in the energy demand and distributed solar power production, Particle swarm optimization (PSO) has resulted in reducing system losses, improving voltage profile, and optimizing the hosting capacity of PVs in balanced networks [7].

Alizadeh et al. [8] have proposed a non-dominated solution-based multi-objective strategy to allocate PVs as efficiently as possible by reducing power loss and improving the voltage profiles for a balanced distribution network. A combined placement index consisting of the loss sensitivity factor and voltage stability factor was formulated for PV placement to reduce the overall network losses and improve the voltage profile [9]. Shaheen et al. [10] have utilized hunter-prey-based algorithms for optimal placement and sizing of PVs in a balanced distribution network to improve the network performance parameters. A hybrid metaheuristic technique comprising of sine-cosine algorithm (SCA) and analytical technique has improved the voltage stability and power losses across the system. The study carefully examined the balanced distribution network [11].

The impact of hourly variations in load demand on the integration of solar systems into the IEEE-14 bus balanced distribution network, considering the PSO and genetic algorithm (GA) for optimum placement and sizing of PVs, has resulted in reducing the power losses and improving the system voltage profile in [12]. An enhanced equilibrium optimizer is proposed to determine the optimum PV placement and size inside the PDNs to minimize the power losses, considering the system constraints [13]. Aref et al. [14] Proposed an approach for allocating solar power generators in balanced power distribution networks in Egypt to lower power loss in the network and improve the voltage profile using PSO and GA optimization techniques. However, the main objective for integrating high-level solar systems in advanced distribution networks is to reduce power loss in the balanced power distribution network [15, 16].

Several approaches to place EVCS optimally have been reported, while each has its own objectives. Comprehensive reviews have been carried out on the integration of EVs and the challenges related to infrastructure, power loss, and environmental impact; and EV charging topologies and power electronic converter (PEC) solutions for EV applications and their impacts on power quality and electric power systems in [17, 18], respectively. As reported in the literature, the integration of EVs into the power system increases the electricity demand [19]. An intelligent algorithm-based approach is employed to solve the planning problem of EVCSs in urban areas to provide a cost-effective and easily accessible EVCS [20]. Nour et al. [21] reported that the distribution network system's peak demand increased by 17.9% when 10% more EVs were added, and by 35.8% when 20% more EVs were added to the system. Higher peak demand from EVs results in higher power losses and voltage fluctuations. This could lead to the overheating of the transformer and the line simultaneously [22]. The use of PSO resulted in the optimal placement of EVCS in the balanced distribution of the system, as reported in [23, 24]. Another hybrid approach, PSO-GWO, has reduced the network power losses of the 33-bus system by 30.67% by optimally placing EVCSs across the radial distribution network [25]. An innovative technique was designed to adjust the size and location of PVs and EVCSs to minimize the undesirable consequences of power quality arising due to their integration into the distribution network by the authors in [26–28]. An optimization control approach integrated with a step-up DC-DC converter has been employed in [29] to enhance the system performance and network efficiency, integrated with solar PV-based EV charging stations.

The integration of PVs and EVCSs results in an increase in power loss and VUF, with the challenge of selecting appropriate sizes and places in the distribution network; hence, deciding on suitable optimization techniques with the objectives of minimizing the power loss and VUF is important. In recent times, BFOA-PSO [30], GA-PSO [31], ECapSa [32], PSO [33], JSO [34], HHO and TLBO [35], and ALO [36] techniques have been considered to minimize power losses and voltage deviation and improve voltage stability while taking into account balanced distribution networks.

The authors of [37–39] offer a novel approach that makes use of optimization techniques to determine the optimal PV unit positions and sizes in association with plug-in electric vehicles (PEVs). The main goal is to minimize energy losses while considering the stochastic nature of PEVs as well as the inherent uncertainty related to PV generation and the dynamic nature of loads. An incentive-based demand side management

of EVs and optimal dispatch of power from distributed generators has resulted in reducing the network power losses by 13.93% [40]. Nandini et al. [41] have implemented JAYA and Whale Optimization Algorithm (WOA) to assess the impact of EVCS and RES on the VUF and power losses on the modified IEEE 33 bus system. A new metaheuristic technique, wild horse optimizer (WHO), has been implemented on the modified IEEE-123 bus system to reduce the active power losses and voltage unbalance with the concurrent integration of PVs and EVCSs [42].

It can be observed from a summary of previous research that the majority of recent studies on the location of PVs and EVCSs in PDNs have concentrated on two main goals: minimizing total energy loss and improving the system's voltage profile. Additionally, the majority of the solutions reported regarding PVs and EVCSs integration in the study were validated on the MV side of the balanced distribution system. However, only a few studies including [43–45] have considered the unbalanced distribution network for the integration of PVs and EVCSs on the LV side of the network [46].

Although the literature covers key components of PVs and EVCSs placement and sizing in balanced and unbalanced distribution networks. However, the impact of PVs and EVCSs on voltage stability, power loss, and VUF in an unbalanced distribution network was overlooked. Assessing the presence of VUF, which can impact network power loss and performance under varying distribution feeder loading conditions throughout the day, was also missing. Henceforth, to fill this gap, a methodology needs to be devised to minimize the maximum APL and VUF over the day. Furthermore, the impact of power losses and voltage unbalance has not been investigated in an unpredictable context with unknown parameters like dynamic load demand, PVs, RESs, and EVs' charging behaviors. Also, the influence of single-phase and three-phase PVs and EVCSs sources placement in unbalanced distribution networks in the context of VUF and APL simultaneously has not been reported. The VUF and APL are also affected by whether PVs and EVs are placed in single or three-phase systems in an unbalanced distribution network. It has been discovered that the VUF on the LV side of the network is not propagated to the MV side of the network, as the distribution transformers across the network are a Dyn vector group.

The current study is unique in that it reduces VUF and APL in an unbalanced distribution network while considering several sources, such as solar PV, EVCS, and dynamic load demand using a metaheuristic technique, Improved Grey Wolf Optimization (IGWO). This work also aims to evaluate and maintain the VUF of an unbalanced real 60-bus system within the stipulated limit of 2% across different cases. The uncertainty in PVs is addressed by taking into account variable and unexpected factors such as solar radiation and the variable states of charge of EVs at EVCS under various limitations. The integration of both single-phase and three-phase PVs and EVCSs has been considered, and an assessment of the VUF and APL of the network has been carried out. It is recommended that the integration of three-phase PVs and EVCSs can aid in converting an unbalanced distribution network into a balanced one, while simultaneously reducing the VUF and APL. The novelty of this research work lies in the application of IGWO for the optimal placement of PV systems within a real unbalanced distribution system incorporating EVCSs. This research work considers the dynamic nature of network load, the intermittent nature of PVs, the stochastic nature of EVs, and their concurrent impact on the hourly variation of APL and VUF on the LV side, which prior research has not examined. IGWO promises superior convergence and optimization efficiency over conventional algorithms. The integrated approach enhances power quality and promotes sustainable network operation by smart integration of REs in unbalanced distribution networks.

The main contributions of this research work are given below:

- Evaluate the effectiveness of single-phase and three-phase PV placement on VUF and APL mitigation.
- Investigate the impact of EVCS charging load on an unbalanced distribution system, considering the stochastic nature of EVs and PVs.
- Investigate the effectiveness of single-phase and three-phase PV and two EVCSs integration in the unbalanced distribution network, for VUF and APL mitigation.

The remainder of the paper is arranged as follows: Section 2 provides details on an unbalanced distribution systems that integrate with renewable energy sources and electric vehicles. Section 3 offers the problem definition and develops the mathematical model of the network under consideration, PV profiles, and EV charging modeling. Section 4 describes the solution procedure using flow charts. Section 5 explains the simulation findings and their comparison. The efficacy of the current study has been established in Section 6, whereas Section 7 summarizes the findings and recommendations for future work.

2 | Problem Statement

Distribution feeders can be categorized based on configuration and load, i.e., radial, loop, and network. Normally, the distribution transformers are operating as unbalanced due to varying loads across each phase of the transformer. Due to this varying nature of the connected load, the unbalancing phenomenon occurs on the LV side of the network, which increases both the VUF and APL of the transformer. The same phenomena exist across all the transformers connected across the distribution feeder. The increased VUF and APL have a negative impact on the distribution network performance and the electrical equipment life. Voltage unbalance can arise in distribution feeders with high PV penetration, non-uniform EV load penetration, and charging patterns over a three-phase system. This study evaluates how the IGWO can be implemented for the strategic position of PVs on the LV side of the network integrated with EVCSs to mitigate the voltage unbalance and power losses in an unbalanced distribution network. Figure 1 illustrates the proposed work, which includes a conventional grid as the primary energy source and solar PV as an alternative source of power for the distribution network and EVCS. The PVs and EVCSs should be strategically placed to compensate VUF and APL across the network.

3 | Problem Formulation

A multi-objective framework is used to analyze the system's APL and VUF across six case studies. The decision variables for

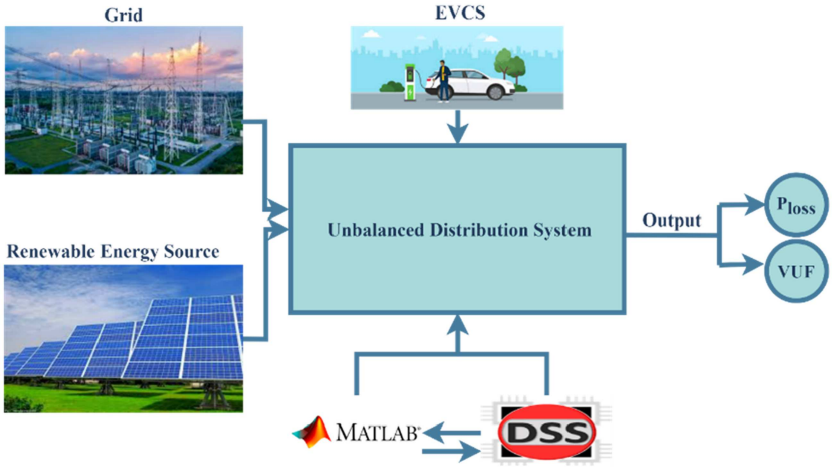

FIGURE 1 | Conceptual view of the proposed work.

PV placement include the location in terms of bus number, size in kW, power factor, and phase selection for PV placement. Similarly, for EVCS, it considers the number of EVs connected at each CS, the location in terms of bus number, the initial SOC of each EV, and the charging schedule of the EVs.

3.1 | Objective Function

The current problem's objective functions are the minimization of APL and VUF.

$$\min_{\theta} F = \alpha f_1 + \beta f_2, \tag{1}$$

where f_1 and f_2 represent the APL and VUF, which are the two objectives of the current study; θ represents the vector of the decision variables. Both objective functions are given equal weightage α and β, i.e., 0.5. Whereas,

$$f_1 = Max\left(\sum_{t=1}^{n_t}\sum_{I=1}^{n_I} P^t_{loss,i} * CP\right), \tag{2}$$

$$P_{loss} = \sum_{S,T=1}^{Br} G_{ST}\left(V_s^2 + V_T^2 - 2V_s V_T \cos\vartheta_{ST}\right), \tag{3}$$

$$f_2 = Max\left(\sum_{t=1}^{n_t}\sum_{I=1}^{n_I} VUF_i^t * CP\right). \tag{4}$$

The equation $P^t_{loss,i}$ represents active power losses in the network at time instant t for state i, with n_t and n_I representing the number of time instants and states, respectively. CP is the combined probability of solar irradiance, EVCS load demand, and the load demand of the network. Br represents the number of branches; G_{ST} denotes the conductance of the line connecting buses S and T.

A small portion of the single-line diagram of a radial distribution system is shown in Figure 2 to calculate the load flow in a radial distribution network. In the figure, two buses are shown; one is the sending end bus designated as bus S, while the receiving end bus is named bus T. The following mathematical

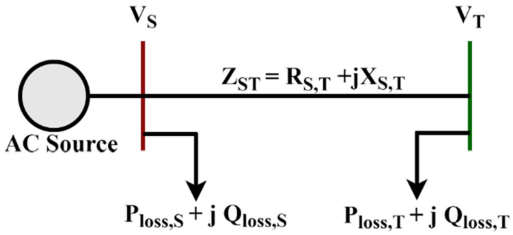

FIGURE 2 | Single Line diagram of Radial Distribution Network.

equations can be used to compute the active and reactive powers across the network:

$$P_S = P_T + P_{L,T} + R_{S,T}\left(\frac{(P_T + P_{L,T})^2 + (Q_T + Q_{L,T})^2}{|V_T|^2}\right), \tag{5}$$

$$Q_S = Q_T + Q_{L,T} + X_{S,T}\left(\frac{(P_T + P_{L,T})^2 + (Q_T + Q_{L,T})^2}{|V_T|^2}\right), \tag{6}$$

where P_S *and*, P_T represent the active power at buses S and T, respectively; and Q_S *and* Q_T, are the reactive power at buses S and T, respectively. $P_{L,T}$ and $Q_{L,T}$ signify the active and reactive load power at bus T. $R_{S,T}$ and $X_{S,T}$ show the series resistance and reactance of the transmission lines S, T, respectively. V_T is the voltage at the bus T and can be computed using the voltage at the bus S (V_S) employing (7):

$$V_T^2 = \left(V_S^2 - 2(P_S R_{S,T} + Q_S X_{S,T}) + \left(R_{S,T}^2 + X_{S,T}^2\right)\frac{\left(P_S^2 + Q_S^2\right)}{V_S^2}\right), \tag{7}$$

Therefore, the active and reactive power losses ($P_{\text{loss}\,(S,T)}$, $Q_{\text{loss}\,(S,T)}$) in the transmission line between buses S and T are computed as:

$$P_{\text{loss}\,(S,T)} = R_{S,T}\left(\frac{P_S^2 + jQ_S^2}{|V_S|^2}\right), \tag{8}$$

$$Q_{\text{loss}\,(S,T)} = X_{S,T}\left(\frac{P_S^2 + jQ_S^2}{|V_S|^2}\right). \tag{9}$$

Hence, the total active and reactive power losses (TPL, TQL) in RDS are computed by aggregating the losses for all branches, Br In the distribution network:

$$TPL = \sum_{S,\mathrm{T}=1}^{Br} (P_{\mathrm{Loss}}(S, T)) \tag{10}$$

$$TQL = \sum_{S,T=1}^{Br} (Q_{\mathrm{Loss}}(S, T)) \tag{11}$$

Two key parameters are to be determined accordingly for each case: VUF and APL over a day. It is essential to compute both the positive and negative sequence components of the voltage for calculating VUF. The (12) and (13) demonstrate the mathematical expression to compute both the positive and negative sequence components of the voltage [47].

$$V_{\mathrm{positive}} = \frac{1}{3} \cdot (V_a + a * V_b + a^2 * V_c), \tag{12}$$

$$V_{\mathrm{negative}} = \frac{1}{3} \cdot (V_a + a^2 * V_b + a * V_c), \quad \& \quad a = 1\angle 120^\circ, \quad a^2 = 1\angle 240^\circ. \tag{13}$$

The VUF is defined in percent as the ratio of the magnitude of the negative sequence voltage to the magnitude of the positive sequence component of the voltage at the fundamental frequency of the system. The mathematical expression is expressed in (14) as:

$$VUF(\%) = \frac{|V_{\mathrm{negative}}|}{|V_{\mathrm{positive}}|} * 100 \tag{14}$$

According to the IEEE standards, the value of VUF on the LV side of the RDS should not exceed 2%. All the scenarios under consideration of the studied system have been simulated, and VUF on LV is calculated accordingly.

3.2 | Constraints

When optimizing an objective function, the technical limitations of the network must be considered. This work has the following equality and inequality constraints for the network under consideration.

3.2.1 | *Equality Constraints*

The total power demand at any instant in time t includes the power demand of the network under consideration, the power demand of EVCS, and the power demand to compensate for the active power losses across the distribution network. The total power demand must be met by the conventional grid and PVs at any instant of time t. In (15), the total power demand is mathematically expressed as

$$P_{grid(t)} + P_{PV(t)} = P_{D(t)} + P_{EVCS(t)} + P_{L(t)}, \tag{15}$$

where $P_{grid(t)}$ represents the power of the grid; $P_{PV(t)}$ shows the power produced by the solar PVs; $P_{D(t)}$ shows the total load demand of the URDS network; $P_{EVCS(t)}$ represents the total power required by the EVCS; $P_{L(t)}$ represent the total active power losses in the distribution network at any instant t of the day.

3.2.2 | *Inequality Constraints*

All bus voltages must be within the minimum and maximum limits, as given in the equation below.

$$V^{\min} \le V_i^t \le V^{\max}, \tag{16}$$

where $V^{\min}$ and $V^{\max}$ indicate the minimum and maximum voltages at bus i, respectively.

$$0.9 \le V_i^t \le 1.1 \tag{17}$$

$$\theta_i^{\min} \le \theta_i \le \theta_i^{\max} \tag{18}$$

$$P_{\min}^{PV} \le P_{i,t}^{PV} \le P_{\max}^{PV} \tag{19}$$

$$I_i^t \le I_{\max} \tag{20}$$

$$S_i^t \le S_{\max} \tag{21}$$

$$\%(VUF)_i \le \%\,(VUF)_{limit} \tag{22}$$

The operational limitations for incorporating PVs and EVCSs in unbalanced distribution networks are multifaceted. To maintain network stability, node voltages must remain within a set range, with each bus's voltage not exceeding upper and lower limitations as defined in (17). Furthermore, in (18), voltage angles at each bus are limited to appropriate values, ensuring that phase angles remain aligned and do not impede power flow. Each PV system provides between 50 and 100 kVA, with a power factor ranging from 0.1 to 1; the highest permitted bus capacity must handle this power output efficiently, as depicted in (19). To minimize overloading, distribution feeders must stay within their rated current limitations in (20), ensuring excessive current does not jeopardize system dependability. Similarly, in (21), distribution lines have a maximum volt-ampere rating that must not be exceeded to ensure safe and effective energy transfer. Finally, to meet regulatory criteria and maintain consistent performance, the VUF is subject to regulation, ensuring that voltage imbalances remain below acceptable limits as defined in (22).

3.3 | Photovoltaic System

Solar irradiance is the primary factor determining PV module output power. PV electricity is unpredictable due to uncontrollable solar irradiation, making forecasting difficult. To model uncertainty, the beta probability distribution function (PDF) is commonly used [48], which represents a bimodal distribution and is expressed as follows:

$$f_{alpha}(\partial) = \begin{cases} \frac{\Gamma(\beta+\gamma)}{\Gamma(\beta)\Gamma(\gamma)} * \partial^{(\beta-1)} * (1-\partial)^{(\gamma-1)} \\ 0, \mathit{Otherwise} \end{cases} , 0 \le \partial \le 1, \beta \ge 0, \gamma \ge 0, \tag{23}$$

where γ represents the solar irradiance in $\frac{kW}{m^2}$ β represent the shape factor parameters of the alpha distribution, which are dependent on the mean μ and standard deviation σ as follows:

$$\gamma = (1-\mu)*\left(\frac{\mu*(1+\mu)}{\sigma^2}-1\right), \tag{24}$$

$$\beta = \frac{\mu*\gamma}{1-\mu}. \tag{25}$$

The *Zth* PV module's power output is calculated in each scenario.

$$P^{PV}_{i,t,z} = \alpha^{PV}*S^{PV}*\partial_{i,t,z}*(1-0.005(T^{am}-25)), \forall_{i,t,z} \tag{26}$$

Here, α^{PV}, S^{PV}, and T^{am} represent the efficiency, surface area, and ambient temperature of PV modules.

3.4 | Electric Vehicle Model

Not all EVs are connected to the distribution network at the same time. The total number of EVs at the CS and their available state of charge (SOC) is determined by the user's daily return time and travel distance per car, which are dependent on driving patterns and charging/discharging preferences for electric vehicles. This research assumes that customers' daily return time and the initially available SOC of every EV are random variables with a normal PDF. Therefore, the daily driving distance is expressed using a logarithmic distribution function as shown below [49]:

$$f_{Dist,k}(v) = \frac{1}{\sqrt{2\pi\sigma_{Dist,t}v}}\exp\left(-\frac{(lnv-u_{Dist,t})^2}{2\sigma_{Dist,t}2}\right) \tag{27}$$

where $\sigma_{Dist,t}$, $u_{Dist,t}$ represent the mean and standard deviation of the distance covered at time t, respectively. After that, to calculate the arrival time of every EV, the normal distribution function is used, as shown below [50]:

$$f_{a,t,k}(t_a) = \frac{1}{\sqrt{2\pi\sigma_{a,t}2}}\exp\left(-\frac{(t_a-u_{a,t})^2}{2\sigma_{a,t}2}\right), \tag{28}$$

where $\sigma_{a,t}$, $u_{a,t}$ denote the mean and standard deviation of the arrival time at t. The average daily return time for EV users is $\mu = 12$ With a standard deviation of 5 h. The EVs are often parked at CSs between 8 and 12 p.m.

$$SoC_{init,k} = \begin{cases} \frac{AMR_k - Dist_k}{AMR_k}, 0 < Dist_k < AMR_k, Dist_k > 0.8*AMR_k, \\ 20\% \end{cases} \tag{29}$$

$$AMR_k = \frac{C_{EVBatt,k}}{E_{\frac{cons}{mile},k}}, \tag{30}$$

Where $Dist_k$ and AMR_k represent the travel distance and all-electric range of the *kth* EV, $C_{EVBatt,k}$ denotes the battery capacity of the *kth* EV, $E_{\frac{cons}{mile},k}$ represents the EV energy consumption per mile.

3.5 | Modeling of EV Battery

At the time instant t, the EV battery's SOC is modified based on charging and discharging, as shown below [37].

$$SoC^{EV}_{i,t,k} = SoC^{EV}_{i,t-1,k} + P^{Ch,EV}_{i,t,k}*\delta^{Ch}_{EV} - \frac{P^{Dc,EV}_{i,t,k}}{\delta^{Dc}_{EV}}, \forall_{i,t,k} \tag{31}$$

where $SoC^{EV}_{i,t,k}$ is the SOC of EV at any time instant t; δ^{Ch}_{EV} and δ^{Dc}_{EV} represent the charging efficiency and discharging efficiency of *kth* EV; and $P^{Ch,EV}_{i,t,k}$ and $P^{Dc,EV}_{i,t,k}$ are the charging power and discharging power of *kth* EV at any time instant t for scenario i, respectively. The percentage of charging power and discharging power for each EV to the overall power of the CS is determined by the battery capacity ($C_{EVBatt,k}$), the current state of charge ($SoC^{EV}_{i,t,k}$), $P_{EVCS,t,i}$, the total power of the CS and t_r the remaining time before departure. To calculate the charging power and discharging power of *kth* EV at time instant t and scenario i, the following relationship is used [51]:

$$P^{Ch,EV}_{i,t,k} = \frac{\left(C_{EVBatt,k} - SoC^{EV}_{i,t,k}*C_{EVBatt,k}\right)*P_{EVCS,t,i}}{t_{r,k}*\sum_{m=1}^{K}\frac{1}{t_{r,m}}\left(C_{EVBatt,m} - SoC^{EV}_{t,m,i}*C_{EVBatt,m}\right)}, \tag{32}$$

$$P^{Dc,EV}_{i,t,k} = \frac{t_{r,n}*\left(SoC^{EV}_{i,t,k}*C_{EVBatt,k}\right)*P_{EVCS,t,i}}{\sum_{m=1}^{M}\frac{1}{t_{r,m}}\left(SoC^{EV}_{t,m,i}*C_{EVBatt,m}\right)}, \tag{33}$$

where $t_{r,k}$ shows the remaining time in EVCS, which can be found from the available data on arrival time $t_{a,k}$ and $t_{d,k}$ departure time as follows:

$$t_{r,k} = t_{d,k} - t_{a,k} \tag{34}$$

The optimization solver determines the total active power of the CS based on the EV batteries' current SOC and departure time.

3.6 | EV Constraints

The EV's power and energy are also limited to ensure its safety when charging. The EV batteries' energy balance is depicted in (35).

$$E^{EV}_{i,t,k} = E^{EV}_{i,t-1,k} + P^{Ch,EV}_{i,t,k}*\delta^{Ch}_{EV}*\Delta T - \frac{P^{Dc,EV}_{i,t,k}*\Delta T}{\delta^{Dc}_{EV}}, \forall_{i,t,k}, \tag{35}$$

Where $E^{EV}_{i,t,k}$ represents the amount of electric energy stored in the *kth* EV at time t. Furthermore, energy storage ought to be limited to a specific range, as defined in (36).

$$E^{EV}_{\min} \le E^{EV}_{i,t,k} \le E^{EV}_{\max}, \forall_{i,t,k}, \tag{36}$$

The charging power is limited to $P^{Ch,EV}_{\max}$, with a binary indicator $Z^{Ch,EV}_{i,t,k}$ showing that the *kth* EV is charging within a certain time period in (37). The discharging power is kept within a maximum of $P^{Dc,EV}_{\max}$, and a binary indicator $Z^{Dc,EV}_{i,t,k}$ indicates that the *kth* EV discharges at a certain time segment t, as shown in (38). The EV's SOC is confined to the $SoC^{EV}_{\max}$ and $SoC^{EV}_{\min}$ limits,

as indicated in (39). However, (40) defines the prohibiting simultaneous charging and discharge [52].

$$0 \le P_{i,t,k}^{Ch,EV} \le P_{\max}^{Ch,EV} * Z_{i,t,k}^{Ch,EV}, \forall_{i,t,k} \quad (37)$$

$$0 \le P_{i,t,k}^{Dc,EV} \le P_{\max}^{Dc,EV} * Z_{i,t,k}^{Dc,EV}, \forall_{i,t,k} \quad (38)$$

$$SoC_{\min}^{EV} \le SoC_{i,t,k}^{EV} \le SoC_{\max}^{EV}, \forall_{i,t,k} \quad (39)$$

$$0 \le Z_{i,t,k}^{Ch,EV} + Z_{i,t,k}^{Dc,EV} \le 1, \forall_{i,t,k} \quad (40)$$

3.7 | Improved Gray Wolf Optimization

Mirjalili introduced the GWO approach in 2014 [53], which replicates the social order and predatory nature of gray wolves. The GWs are well-designed to be the top predators in the food chain, while the approach is simple, easy to grasp, and requires few parameter adjustments. Wolves' hunting strategy involves three phases: approaching, surrounding, and attacking the prey. Every gray wolf represents a potential replacement in the population.

The GWO approach categorizes the wolves into four distinct levels: α; representing the current best individual and presents the finest option, β and δ; the inferior second and third-best options, and ω; representing the conventional alternative, while $\alpha > \beta > \delta > \omega$. The GWs encircle the prey, as shown in (41) and (42).

$$\vec{G} = |\vec{F} \times \vec{Y}_p(t) - \vec{Y}(t)| \quad (41)$$

$$\vec{Y}(t+1) = \vec{Y}_p(t) - \vec{E} \times \vec{G} \quad (42)$$

$\vec{Y}(t)$, $\vec{Y}_p(t)$, and t demonstrate the current positioning vector of the GW, the position of the prey, and *tth* iteration correspondingly. The vectors $\vec{E}$ *and* $\vec{F}$ are explained in detail in (43).

$$\vec{E} = 2\vec{v}\,\vec{m_1} - \vec{v}, \vec{F} = 2\vec{m_2} \quad (43)$$

Where $\vec{m_1}$ and $\vec{m_2}$ are random vectors that range from 0 to 1. In (42), it is explained how the elements of $\vec{v}$ decrease linearly from 2 to 0 over iterations.

$$\vec{v} = 2 - \frac{2 \times t}{t_{\max}} \quad (44)$$

It is assumed that $\alpha, \beta,$ *and* δ, have a better understanding of the prey's location. As a result, wolves ω are obliged to track $\alpha, \beta,$ *and* δ. The hunting activity is described in (45).

$$\begin{aligned} \vec{G_\alpha} &= |\vec{F_1} \times \vec{Y_\alpha} - \vec{Y}(t)|, \\ \vec{G_\beta} &= |\vec{F_2} \times \vec{Y_\beta} - \vec{Y}(t)| \vec{G_\delta} = |\vec{F_3} \times \vec{Y_\delta} - \vec{Y}(t)| \end{aligned} \quad (45)$$

The coefficients $\vec{F_1}$, $\vec{F_2}$, and $\vec{F_3}$ can be calculated as shown in (41). The top three solutions at the *tth* iteration are referred to as $\vec{Y_\alpha}$, $\vec{Y_\beta}$, and $\vec{Y_\delta}$. Similarly, the vectors $\vec{E_1}, \vec{E_2}$, and $\vec{E_3}$ are calculated as mentioned in (43).

$$\begin{aligned} \vec{Y_{i1}} &= \vec{Y_\alpha} - \overrightarrow{E_1 \times} (\vec{G_\alpha}), \vec{Y_{i2}} = \vec{Y_\beta} - \overrightarrow{E_2 \times} (\vec{G_\beta}), \vec{Y_{i3}} \\ &= \vec{Y_\delta} - \overrightarrow{E_3 \times} (\vec{G_\delta}) \end{aligned} \quad (46)$$

$$\vec{Y}_{i-GWO}(t+1) = \frac{\vec{Y_{i1}}(t) + \vec{Y_{i2}}(t) + \vec{Y_{i3}}(t)}{3} \quad (47)$$

The wolves attack the prey when they halt, ending the hunt. This can be mathematically represented as a linear decrement throughout the iteration process that controls intensification and diversification. This GWO has a wide range of uses. However, it has drawbacks such as an absence of population variance, a disparity within intensification and diversification, trouble coming up with workable solutions, and early convergence. The IGWO technique was used in the present study to address the issue effectively. The process involves three stages: initialization, movement, and selection/update.

Initializing the population: Throughout this stage, N wolves are distributed arbitrarily around the search territory, which has dimensions D and lies within the defined range; $[l_i, u_k]$ described in (46). $t_{\max}$ indicates the highest number of iterations.

$$\vec{Y}_{ik} = l_k + \text{rand}_k\,[0,1] \times (u_k - l_k), i \in [1,N], k \in [1,G] \quad (48)$$

The GW population is randomly initialized between several power grid variables. The position of the ith wolf in *tth* iteration is represented as $\vec{Y}_i(t) = \{\vec{Y_{i1}}, \vec{Y_{i2}}, \cdots\cdots, \vec{Y_{iD}}\}$. The Population matrix $(N \times G)$ retains the entire wolf population.

Movement phase: The research IGWO employs an agile technique known as a learning-based hunting dimension (LHD) search. Within LHD, each wolf is trained by its neighbor wolves to pretend to be an option for $Y_i(t)$'s new position. Two distinct options are produced by the GWO and LHD techniques. Each dimension of a wolf's position $\vec{Y}_i(t)$ is assessed using the LHD method, allowing them to learn from their neighbors and a randomly selected wolf from Pop. In addition to $\vec{Y}_{i-GWO}(t+1)$, the LHD approach generates another candidate, $\vec{Y}_{i-LHD}(t+1)$, regarding the newly created position. To evaluate a radius $\vec{R}_i(t)$, calculate the Euclidean distance from $\vec{Y}_i(t)$to the position candidate's $\vec{Y}_{i-GWO}(t+1)$, as demonstrated in (49):

$$\vec{R}_i(t) = \|\vec{Y}_i(t) - \vec{Y}_{i-GWO}(t+1)\| \quad (49)$$

To find the neighbors of $\vec{Y}_i(t)$ use (50) and radius $\vec{R}_i(t)$,where $\vec{G}_i$ denotes the Euclidean distance between $\vec{Y}_i(t)$ and $\vec{Y}_j(t)$. A multi-neighborhood learning is represented in (51) when building a community around $\vec{Y}_i(t)$.

$$\vec{N}_i(t) = \{\vec{Y}_j(t) | \vec{G}_i(\vec{Y}_i(t), \vec{Y}_k(t)) \le \vec{R}_i(t), \vec{Y}_k(t) \in \text{Pop}\} \quad (50)$$

To determine the *dth* dimension of $\vec{Y}_{i-LHD,g}(t+1)$, the *dth* dimension of a random neighbor $\vec{Y}_{n,g}(t)$ from $\vec{N}_i(t)$ and a single wolf $\vec{Y}_{m,g}(t)$ chosen at random from the Population is used.

$$\vec{Y}_{i-LHD,g}(t+1) = \vec{Y}_{i,g}(t) + \text{rand} \times (\vec{Y}_{n,g}(t) - \vec{Y}_{r,g}(t)) \quad (51)$$

Select and update the GWs' locations: This stage entails encircling and attacking the target. The fitness values of $\vec{Y}_{i-GWO}(t+1)$ and $\vec{Y}_{i-LHD,g}(t+1)$ are compared using (52) to p ropose the candidate with the highest fitness score. After surrounding the prey, GWs α, β, and δ had a clearer understanding of its location.

$$\vec{Y}_i(t+1) = \begin{cases} \vec{Y}_{i-\mathrm{GWO}}(t+1), iff\ (\vec{Y}_{i-\mathrm{GWO}}) < f(\vec{Y}_{i-LHD}) \\ \vec{Y}_{i-LHD}(t+1) \text{otherwise} \end{cases} \quad (52)$$

To update the procedure to the new position labeled $\vec{Y}_i(t+1)$, two criteria must be met: if the fitness value of the selected candidate is less than $\vec{Y}_i(t)$, ultimately $\vec{Y}_i(t)$is advanced by the selected candidate, otherwise $\vec{Y}_i(t)$ remains unchanged in the Population matrix. Lastly, the iteration number is incremented until it is attained. The sequence of steps used in the current study, based on IGWO to find the optimal solution, is described in Figure 3.

3.8 | Co-Simulation of MATLAB and OpenDSS

The suggested approach has been tested on a real Pakistani distribution system (the 60-bus distribution system) to show how successful it is. The data of the network under consideration has been accessed using the Open Distribution System Simulator (OpenDSS) package, a distribution system simulator (DSS) by EPRI designed for smart grids and renewable energy [54].

MATLAB® R2021b is used to test the simulation framework on a laptop equipped with a 2.60 GHz Intel® Core i7-6600U processor and 16 GB of main memory. This study uses OpenDSS for power system modeling, PV unit modeling, EV modeling, power flow analysis, and smart inverter control. The unbalanced distribution system is simulated and computed using OpenDSS. More specifically, we use MATLAB® to manage the OpenDSS using a component object model (COM) interface that allows us to adjust load, transformer, and line parameters, as well as analyze power-flow solutions. OpenDSS always awaits the commands from MATLAB. When a command is sent to OpenDSS from MATLAB, it is executed and, if any results are obtained, returned to MATLAB. This method is performed for every command that OpenDSS must execute. Figure 4 depicts a generic structure for implementing our suggested technique in the MATLAB®-OpenDSS co-simulation environment. MATLAB only supports matrix arithmetic, conditional branching, looping, and communication with OpenDSS.

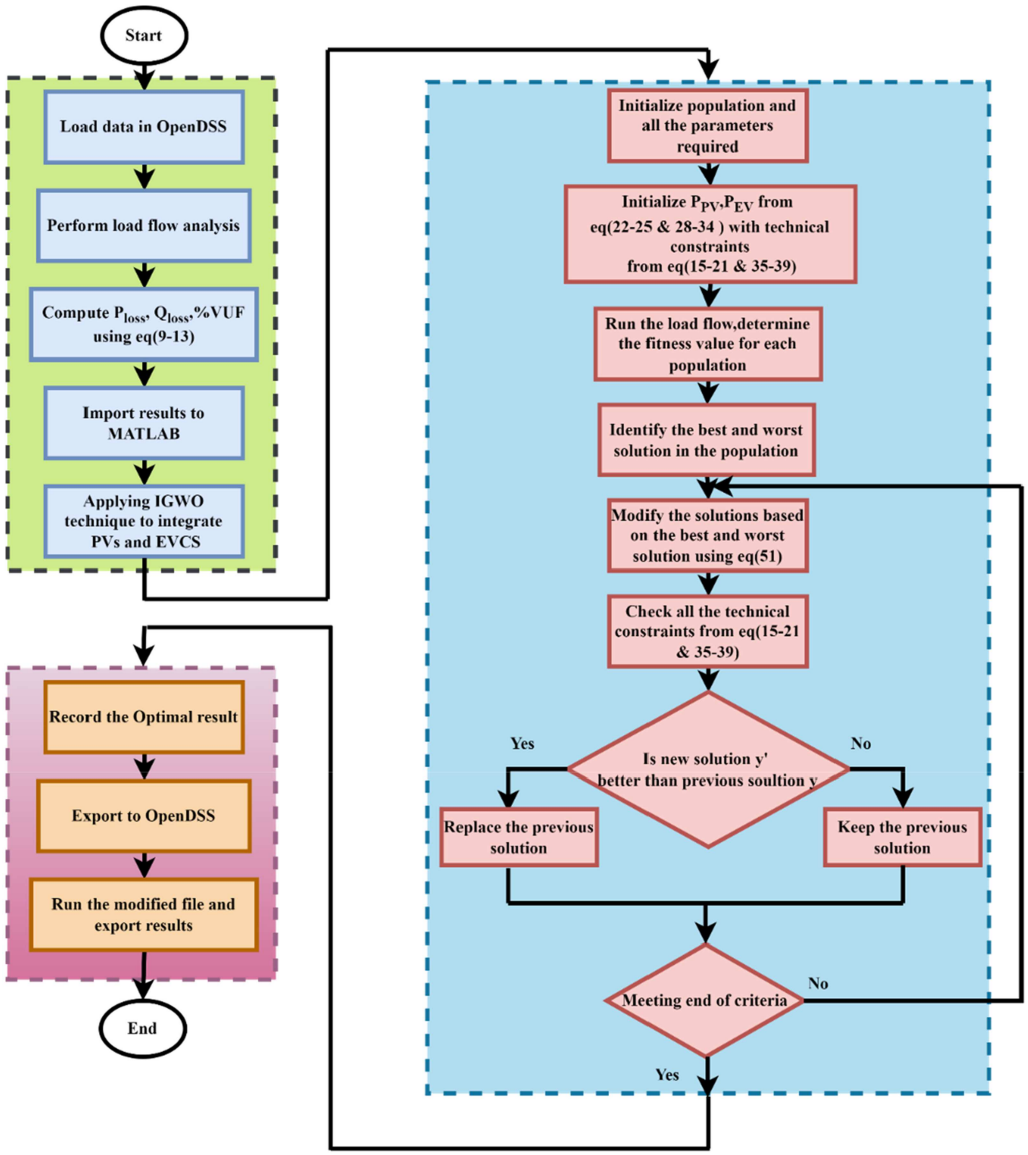

FIGURE 3 | Flowchart of the proposed methodology for the Optimal solution using IGWO.

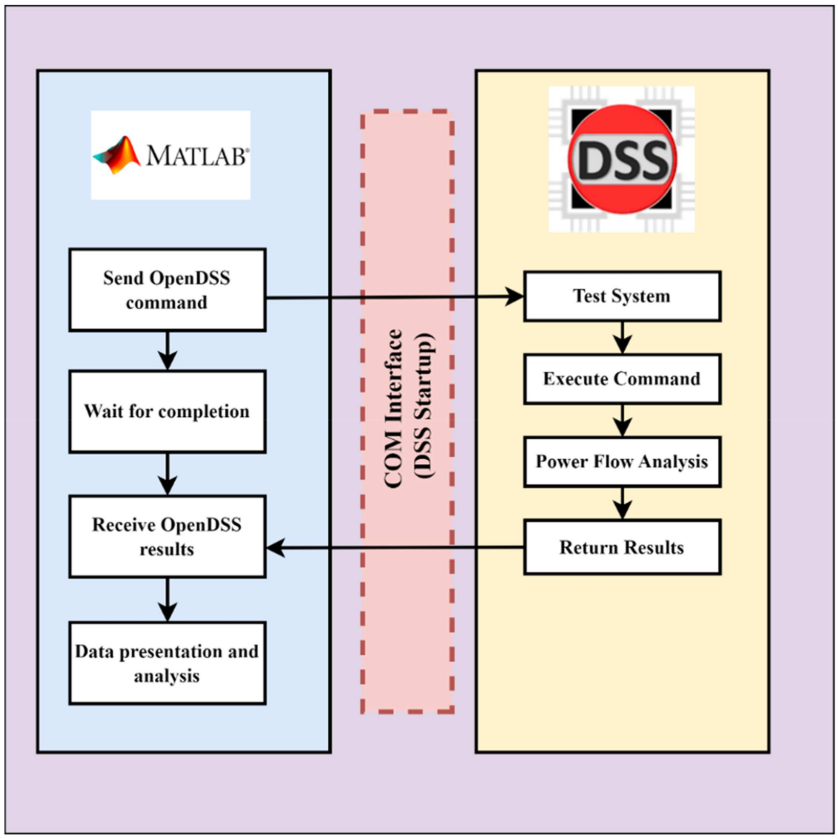

FIGURE 4 | Interfacing OpenDSS and MATLAB.

Whereas OpenDSS analyzes a system's power flow 24 times for each potential solution. The proposed method's performance is then validated through a variety of case studies.

4 | Case Study

The proposed methodology is implemented to evaluate its effectiveness on the standard 11 kV Real-60 Bus unbalanced RDS (URDS) system on the LV side for the optimal sizing and placement of PVs and EVCSs using IGWO. This work aims to create a different set of cases and, through a detailed analysis, draw a general conclusion on how these PVs and EVCSs impact the power quality aspects of an unbalanced distribution network. The following case studies have been created to examine the performance under different conditions.

4.1 | Case-I: Without Compensation

The base case scenario analyzes a real 60-bus system under normal operating conditions, implying that no PVs or EVCSs are integrated into the network. Both the APL and VUF are calculated over a day, and the maximum values of both parameters are recorded.

4.2 | Case-II: Single-Phase PVs Integration

In this case, single-phase PVs are integrated at the optimal locations into the network under consideration using IGWO. The maximum values of APL and VUF are observed over a daytime.

4.3 | Case-III: Three-Phase PVs Integration

Three-phase PVs are incorporated at the optimal locations across the network under consideration using IGWO in this case, whereas APL and VUF are also evaluated and analyzed.

4.4 | Case-IV: 2 Evcs Integration in G2V Mode

Two EVCSs are configured at the specific locations across the network, and the Grid to Vehicle (G2V) mode is activated for the current case.

4.5 | Case-V: Single-Phase PVs and 2 Evcs Integration

Two EVCSs in G2V mode are connected at fixed locations across the network, and single-phase PVs are integrated at the optimum locations into the network using IGWO.

4.6 | Case-VI: Three-Phase PVs and 2 EVCS Integration

In this case, two EVCSs and three-phase PVs are integrated into the network under consideration at their optimal locations using IGWO.

Each case study is simulated and analyzed for 24 h over a day with a time interval of 1 h. APL and VUF are calculated over a day. The designed network is a real 60-bus system URDS. Out of 60 buses, 59 buses are load buses. The transformers, Dyn type,

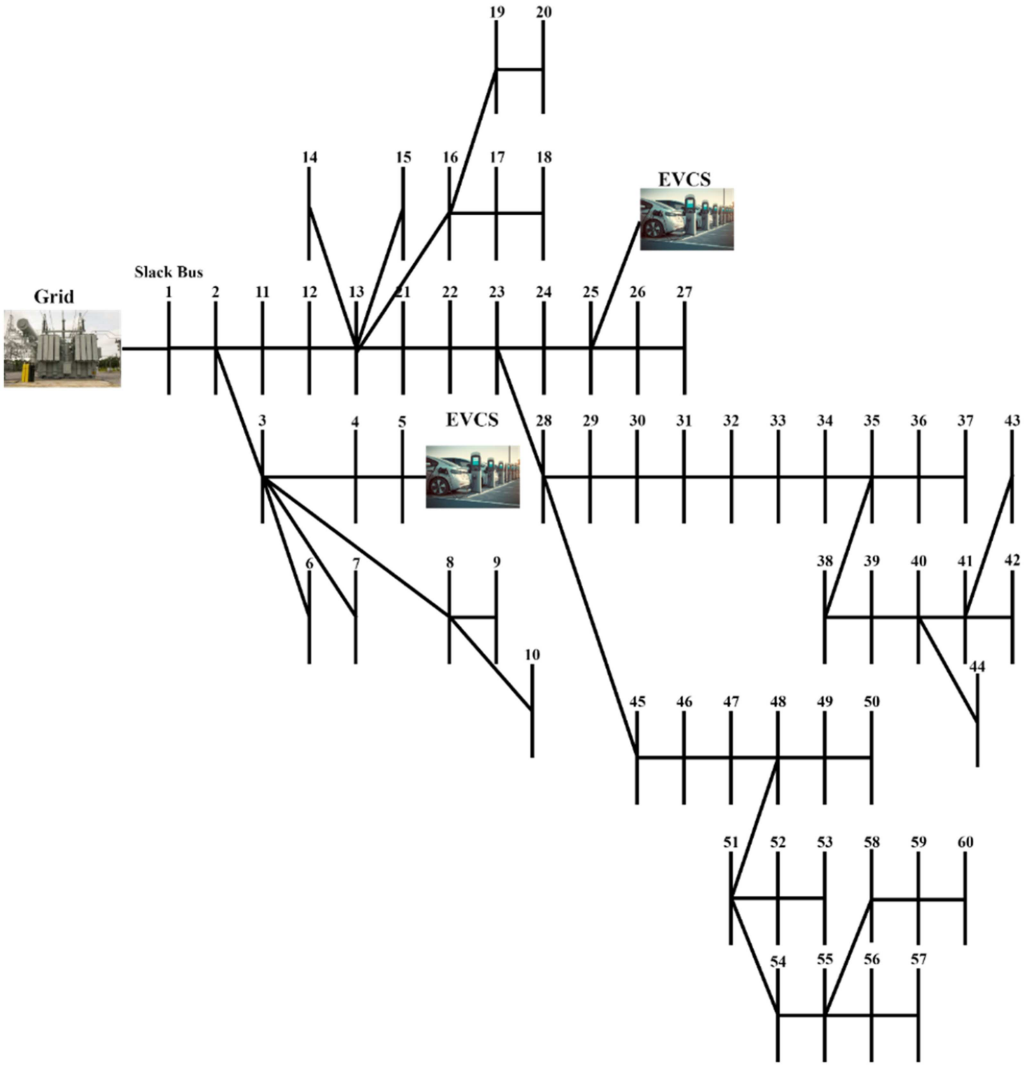

FIGURE 5 | Real 60-Bus Unbalanced Radial Distribution Network.

with different capacities ranging from 25 kVA to 400 kVA, are connected in the network. The network under consideration is 11/0.415 kV, whereas Figure 5 shows the real 60 bus URDS under consideration.

The URDS network is outlined in Table 1 for the considered real 60-bus system. The distribution network requires a total of 7.21 MW of active power and 1.768 MVAR of reactive power, respectively, whereas the network's line voltage is 11 kV. The voltage magnitude of each phase, phase angle, and power losses are calculated accordingly.

TABLE 1 | Real 60 Bus URDS Total Power Demand.

Parameters	Values	
Bus type	Real 60-Bus	
Active power (MW)	7.2	
Reactive power (MVAR)	1.768	
Apparent power (MVA)	7.41	
Voltage level (kV)	11/0.415	
Transformers	**No. of T/Fs**	**Size (kVA)**
	6	25
	10	50
	20	100
	22	200
	1	400

5 | Results and Discussion

5.1 | Case-I: Without Compensation

In the current case, there is no integration of any PVs and EVCSs along the network under consideration. The system under consideration is simulated, and the voltage magnitude, active power losses, and VUF are calculated, respectively. The voltage magnitude decreases at the end of the feeder due to its radial nature. As a result, the consumer at the end of the feeder faces LV issues. This can lead to economic and power quality concerns, such as line losses, reliability, and stability. The actual maximum active power losses of the network, calculated using Open DSS load flow analysis, are 455.472 kW at the 17th hour of the day within the URDS as presented in Figure 6. Additionally,

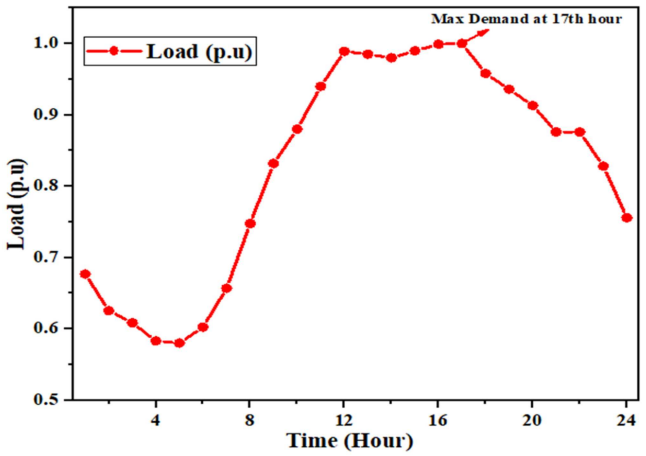

FIGURE 6 | Demand Curve over a day.

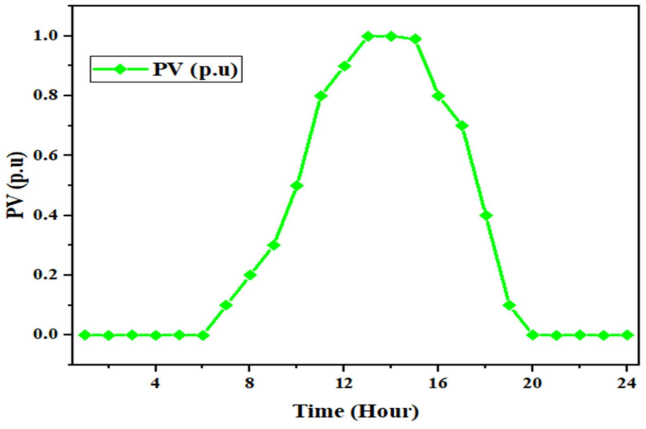

FIGURE 7 | PV power curve over a day.

the maximum value of VUF observed is 2.02% at the 17th hour of the day. As observed from Figure 6, the load demand is maximum at the 17th hour of the day which also resulted in the maximum values of APL and VUF at the same hour of the day.

5.2 | Case-II: Single-Phase PVs Integration

Single-phase PVs are integrated into the URDS at the optimum location on the LV side using IGWO. It provides power during the daytime as solar power generation depends upon the solar irradiation available. The end user consumers install PVs to produce their electricity, reducing their dependence on the conventional grid, and helping the users to reduce their electricity bill costs. Figure 7 shows the PV power profile over a day.

Integrating solar PVs can help to reduce active power losses and VUF. It can be observed from Figure 8 that the PV profile and demand curve overlap from the 7th hour of the day to the 18th hour of the day. It has been observed that maximum APL increased up to 474.860 kW at the 17th hour of the day, and the value of VUF increased from 2.02% to 2.46%. As long as single-phase PVs are supplying power to the URDS, both the APL and VUF increase.

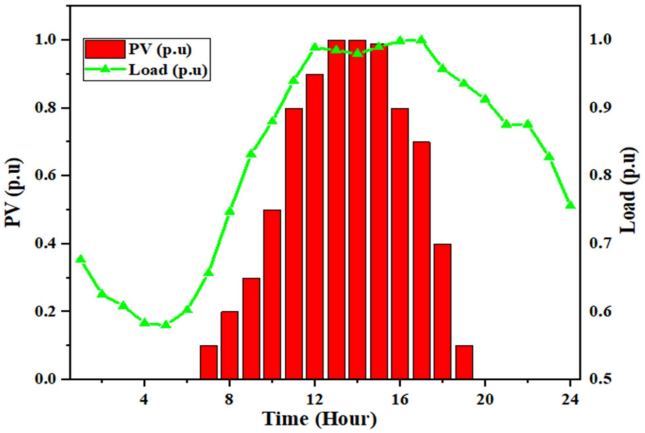

FIGURE 8 | Overlapping curve of PV profile and load profile.

5.3 | Case-III: Three-Phase PVs Integration

Three-phase PVs are installed in the under-consideration URDS at optimum locations across the network. With the integration of the PVs, it was observed that the maximum values of APL decreased from 455.472 kW to 338.826 kW at the 17th hour of the day. Similarly, the value of VUF also reduced from 2.02% to 1.91% at the 17th hour of the day.

5.4 | Case-IV: 2 EVCS Integration in G2V Mode

When EVCS is integrated into the distribution network in G2V mode, EVs receive electric power from the conventional grid to charge their battery. This mode of charging is called the "charging mode or grid mode". The EVCS operated as the linkage between the grid and the EV in this mode. As the CS is connected to the grid, it receives power, converted to specific voltage and current levels as per the standard of EV battery charging.

This charging mode or grid mode increases the APL in the network due to the additional load of two CSs of 1564 kW each with a capacity of 782 kW. The optimal location of both EVCSs is at the 5th and 25th buses of the distribution network. The size and location of EVCSs within the distribution network have a negative impact on the power losses, VUF, and voltage profile if not placed at optimum locations. Figure 9 shows the EV profile at the CS over the day. As the maximum number of EVs is available at the CS for charging from 7th to 12th hour of the day, the network requires extra power from the grid to meet these EVCS loads. It has been observed that the maximum APL has increased from 455.472 kW to 506.286 kW from the 17th hour of the day to the 11th hour of the day. The results also reflect that VUF increases from 2.02% to 2.06% from the 17th hour of the day to the 12th hour of the day.

5.5 | Case-V: Single-Phase PVs and 2 EVCS Integration

Integrating EVCSs and PVs optimally into the distribution network can be beneficial for both the end users and the grid. The end users can avail benefits of PVs to produce their electricity, reducing the burden on the conventional grid and helping the consumers save their utility bills. In the current case, single-phase PVs are optimally placed across the LV side of the network. As most EVs are available in the CS from the 7th to 12th hour of the day, solar

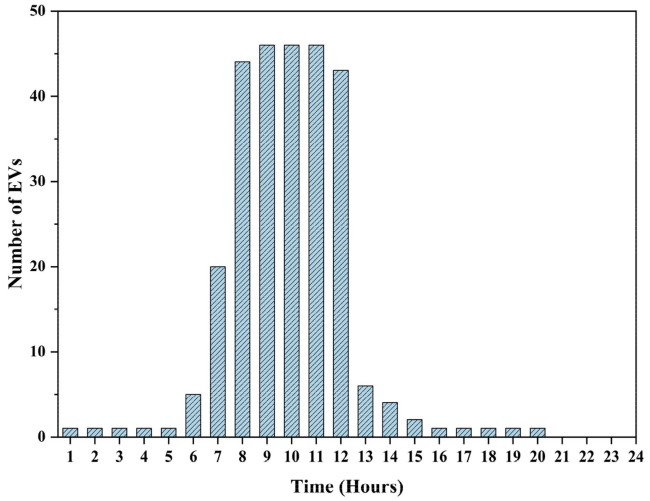

FIGURE 9 | Number of EVs at EVCS over a day.

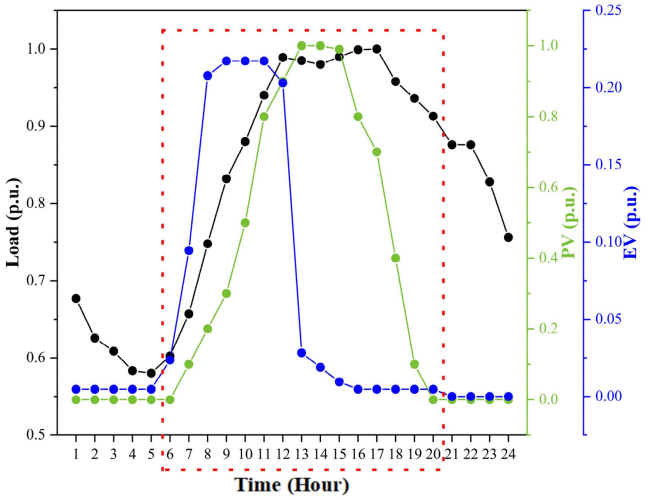

FIGURE 10 | Overlapping interval of EVs, PVs, and the demand curve.

power is also contributing to the network during the same hours, which has also been highlighted in Figure 10. This single-phase PV integration further increases the network APL and VUF simultaneously during these hours of the day. The power loss increases from 455.472 kW to 537.668 kW. Moreover, the maximum power loss shifts from the 17th hour of the day to the 11th hour of the day. It is clear from the figure that the overlapping interval of EVs, PVs, and demand curves is from the 7th to 12th hour of the day. Integrating two EVCSs with single-phase PVs has an adverse impact on both the APL and VUF. The maximum value of the VUF is 2.46% at the 19th hour of the day.

5.6 | Case-VI: Three-Phase PVs and 2 EVCS Integration

When the distribution network is integrated with three-phase PVs, though it reduces the burden on the grid due to the extra load of two EVCSs, it lessens the load on the conventional grid by supplying balanced three-phase power across the LV side of the network. In this mode, EVCSs are optimally placed at the 5th and 25th buses of the distribution network. Three-phase PVs are optimally positioned at the optimum location across the network on the LV side. This also promotes sustainability and reduces the maximum APL across the network from 455.472 kW to 387.949 kW at the 11th hour of the day. VUF also reduces from 2.02% to 1.94% from the 17th hour of the day to the 12th hour of the day. Integrating three-phase PVs helps to reduce APL and VUF across the network even when two EVCSs are present in the distribution network.

This research work explains the in-depth systematic analysis of an unbalanced distribution network, highlighting power quality issues like VUF and APL. Also, analyzing the impact of PVs and EVCSs integration on the URDS network performance, either alone or in combined operation. Six different cases were defined to assess the impact of PVs and EVCSs on the value of VUF and APL over a day. Figures 11 and 12 compare the APL and VUF for all the cases under consideration over 24 h of the day. It can be observed from Case I that the maximum value of the load on the demand curve was at the 17th hour of the day. Resultantly, the maximum value of APL 455.472 kW and VUF 2.02% was observed at the 17th hour of the day. Case II considered the optimal placement of single-phase PVs across the LV side of the

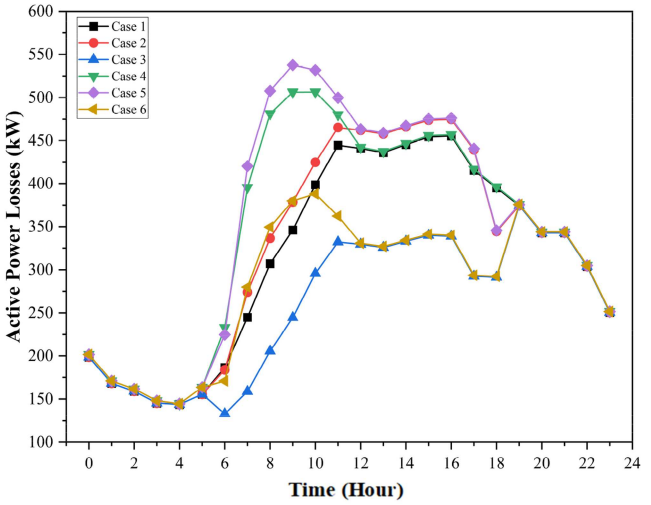

FIGURE 11 | Comparison of active power loss values over a day for all cases.

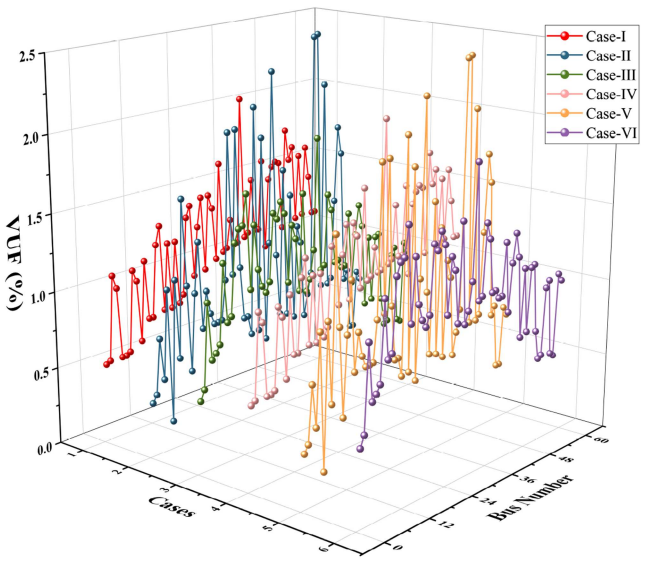

FIGURE 12 | Comparison of VUF across the URDS for all cases.

network. The load demand curve and PV power profile overlap from the 7th to the 19th hour of the day. Whereas both the maximum value of VUF and APL had increased by 21.78% and 4.25% at the 17th hour of the day, as compared to Case-I. The Case-II results gave the understanding that single-phase PV integration increased both the VUF and APL, as observed in [46, 55]. Single-phase PV integration in URDS tries to improve the voltage magnitude of that phase at the cost of deteriorating the voltage profile of other phases, hence leading to an increase in VUF. As observed in Figures 11 and 12, due to the single-phase PV integration, APL and VUF have increased as compared to Case-I.

TABLE 2 | Performance of Real 60-bus URDS Under Different Cases.

Cases		Items	IGWO
Case-I	Without compensation	Max P_{loss} (kW)	455.472
		Max VUF (%)	2.02
		Vmin (p.u)	0.9107
		Energy Loss over a day (MWh/day)	7.65
Case-II	With single phase PVs	PVs (Solar) size in kW	2977
		Max P_{loss} (kW)	474.860
		%P_{loss} increase	4.25
		Max VUF (%)	2.46
		%VUF increase	21.78
		Vmin (p.u)	0.9191
		Energy Loss over a day (MWh/day)	7.76
Case-III	With three phase PVs	PVs (Solar) size in kW	3070
		Max P_{loss} (kW)	338.826
		%P_{loss} decrease	25.6099
		Max VUF (%)	1.91
		%VUF decrease	5.44
		Vmin (p.u)	0.9230
		Energy Loss over a day (MWhr/day)	6.2
Case-IV	With 2 EVCS(G2V) mode	EVCS size in kW (Location)	782 (5), 782 (25)
		Max P_{loss} (kW)	506.286
		%P_{loss} increase	11.15
		Max VUF (%)	2.06
		%VUF increase	1.98
		Vmin (p.u)	0.9090
		Energy Loss over a day (MWh/day)	8.26
Case-V	With 2 EVCS and single-phase PVs	EVCS size in kW (Location)	782 (5), 782 (25)
		PVs (Solar) size in kW	2977
		Max P_{loss} (kW)	537.668
		%P_{loss} increase	18.04
		Max VUF (%)	2.46
		%VUF increase	21.78
		Vmin (p.u)	0.9116
		Energy Loss over a day (MWh/day)	8.46
Case-VI	With 2 EVCS and three phase PVs	EVCS size in kW (Location)	782 (5), 782 (25)
		PVs (Solar) size in kW	3070
		Max P_{loss} (kW)	387.949
		%P_{loss} decrease	14.82
		Max VUF (%)	1.94
		%VUF decrease	3.96
		Vmin (p.u)	0.9220
		Energy Loss over a day (MWh/day)	6.8

Case III highlights the importance of three-phase PV integration into URDS. Three-phase PV integration injects balanced power across the LV side of an unbalanced distribution transformer, which accumulatively improves the system performance by reducing the maximum APL and VUF by 25.60% and 5.44% across the URDS as compared to Case-I. The Case-IV elaborates on the optimal placement of two EVCS in the URDS under consideration. The maximum number of EVs was at the CS from the 7th to the 12th hour of the day. The power demand of these EVCSs was met by the conventional grid, leading to an increase in both the maximum APL and VUF by 11.15% and 1.98% simultaneously in comparison to Case-I. Since the network power demand was small from the 7th to the 12th hour of the day, the excessive power demand of EVCSs shifted the maximum APL and VUF of the network from the 17th hour of the day to the 12th hour of the day. Moreover, it was observed that integrating two EVCSs into the network resulted in an increase in network losses. Hence, to reduce the impact of EV charging on the conventional grid, it is always recommended to add energy sources.

The Case-V considered the combination of optimal placement of EVCSs and single-phase PVs in the network under consideration. Due to the inclusion of EVCS, the APL and VUF of the network increased as observed in Case IV. The single-phase PV integration with EVCS further increased the APL and VUF. As evident from Figure 10, the overlapping interval of EV charging, PV power curve and demand curve of the network was from the 7th to the 12th hour of the day. This single-phase PV integration must support reducing the burden on the conventional grid by power-sharing due to the excessive load demand of EVCS. But instead of power support from PVs, the maximum APL and VUF of the network increased by 18.04% and 21.78% at the 11th hour of the day.

The Case-VI considered the optimal placement of EVCSs and three-phase PV integration simultaneously for the network under consideration. It can be judged from Figures 11 and 12 that the maximum value of the APL and VUF decreases by 14.82% and 3.96% at the 12th hour of the day. Since both the APL and VUF of the URDS are directly linked to each other, henceforth the three-phase PV integration injected balanced power into the bus, which reduced the voltage imbalance between the phases at that bus and resulted in a reduction in power losses across the same bus. The PVs were optimally placed across the whole network, and the contribution of all these PVs led to a reduction in the APL and VUF of the network.

Table 2 compares all six cases, as observed Case-VI and Case-III can be considered the best choices among the all cases studied, whereas Case-V seems to be the worst case.

Figure 13 shows the comparison of active energy loss over a day and the maximum value of VUF for all the cases under consideration. It has been observed that no matter what the case is, single-phase PVs integration have an adverse impact on the voltage unbalance and power losses. The analysis of all cases clearly explains that to minimize the VUF and APL, it is highly recommended to integrate three-phase PVs and EVs into the unbalanced distribution network. In the current distribution system, most of the end user loads are single-phase and have acquired single-phase electricity connection from the utility. Whereas most of the LV networks in the current distribution network have three phases and end users have easy access to all three phases in their vicinity. Hence, based on our findings, it is recommended that forcing the end users to go for three-phase electricity connections and upgrading the existing single-phase users to three-phase in order to minimize the unbalancing situation, to maximize the hosting capacity of PVs and EVs in URDS.

6 | Comparative Evaluation and Scalability of IGWO on IEEE−123 Bus System

To verify the efficacy and scalability of the proposed methodology to integrate PVs and EVCSs on the LV side of the network using IGWO, the IEEE−123 bus system is considered. The results are compared with the other optimization techniques and are tabulated in Table 3, showing that integration of three-phase PV and

TABLE 3 | Performance Comparison of PSO, ABC, ALO, and IGWO Against Base Case on IEEE−123 Bus System.

Applied Methods	DG Size	Phase	Vmax	Vmin	Max P_{loss} (kW)	Max VUF (%)	Energy Loss (MWh/day)
Base Case	—	A	1.0508	0.9766	95.0	1.0623	1.28
		B	1.0477	0.9789			
		C	1.0496	0.9789			
PSO [33]	1255	A	1.0478	0.9807	77.9	0.9593	1.02
		B	1.0478	0.9813			
		C	1.049	0.9819			
ABC [56]	1102	A	1.0519	0.9807	77.5	0.9492	1.10
		B	1.0516	0.9828			
		C	1.0533	0.9828			
ALO [36]	1493	A	1.046	0.9805	77.7	0.9475	0.91
		B	1.0477	0.9823			
		C	1.0489	0.9827			
IGWO [57]	1430	A	1.0484	0.9806	77.5	0.9466	0.87
		B	1.0478	0.9807			
		C	1.0489	0.9816			

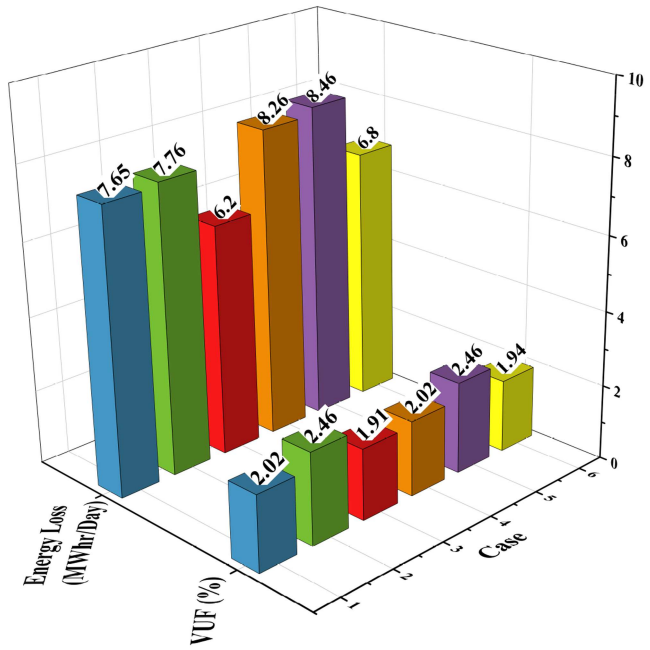

FIGURE 13 | Energy Loss (MWh/day) and VUF Over a Day.

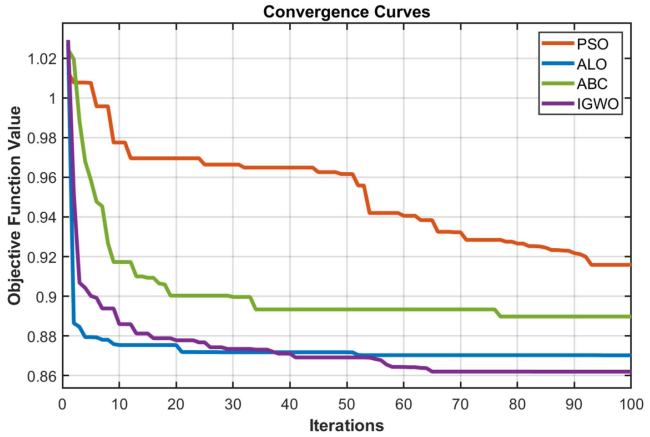

FIGURE 14 | Convergence curves of PSO, ALO, ABC, and IGWO for Case VI.

EVCSs on the LV side of the IEEE−123 bus system has led to a reduction of both VUF and energy loss over a day. Whereas the IGWO has outperformed other mentioned techniques in terms of improving the network performance.

The convergence behavior of the recommended IGWO methodology has been examined with other established methods, including particle swarm optimization (PSO), ant lion optimization (ALO), and artificial bee colony (ABC), for Case VI in order to further demonstrate the effectiveness of the optimization technique. Figure 14 shows the evolution of the objective function values over iterations, giving a visual representation of the patterns of convergence.

7 | Conclusion

This research suggested a way to reduce the LV network VUF and APL by integrating three-phase PVs and EVs into an unbalanced distribution network. The suggested method offers rooftop PVs and EVCSs placement and sizing solutions that maximize system performance while maintaining operational limitations like node voltages, branch currents, feeder loading capacity, VUF, and APL. The model was developed as a mixed-integer nonlinear multi-objective optimization, with the objectives of minimizing the VUF and APL in a real 60-bus Pakistani URDS. The IGWO technique was used to solve this multi-objective model to determine the best solution, ensuring that no objective function outweighs the others. The simulation results show that optimal placement and sizing of three-phase PVs and EVCSs helped to maximize the penetration level of PVs and meet the varying EV demand in the network. According to the simulation results, integrating three-phase PVs with EVCS reduced the APL and UVF by 14.82% and 3.96% while integrating single-phase PVs and EVCSs increased APL by 18.04% and VUF by 21.78% in a real 60-bus URDS.

While carrying out the current study, Total Harmonic Distortion (THD) was not considered, which arises due to the integration of the PVs and EVCSs, and EVs V2G mode for peak load management, which will be the aim of our future study. Moreover, in the future, other energy resources such as wind energy, fuel cells, compressed air energy storage, and hydrogen storage will also be integrated and their impact on the URDS will be analyzed.

Indices and sets

K	Index of EV
Z	index of PV
t	Index of time
I	Index of scenario

Parameters

AMR_k	All-electric range for the kth EV
$E_{\frac{cons}{mile},k}$	Energy consumption per mileage of the kth EV
$E^{EV}_{\min}/E^{EV}_{\max}$	Min/Max energy limit of the EV's battery
$\delta^{Ch}_{EV}/\delta^{Dc}_{EV}$	Charging and discharging efficiencies of the EV
$SoC^{EV}_{\min}/SoC^{EV}_{\max}$	Min/Max SOC limits of the EV
$E^{EV}_{i,t,k}$	Energy content of the EV's battery in kWh
$P^{Ch,EV}_{i,t,k}/P^{Dc,EV}_{i,t,k}$	Charging/discharging power of the EV in kW
$P_{EVCS,t,i}$	EVCS power in kW
$SoC^{EV}_{i,t,k}$	State of charge of the EV
$Z^{Ch,EV}_{i,t,k}/Z^{Dc,EV}_{i,t,k}$	Charging and discharging binary variables of the EV

Author Contributions

Maaz Ahmad: conceptualization, data curation, investigation, methodology, visualization, writing – original draft. **Aamir Nawaz:** formal analysis, investigation, writing – review and editing. **Rahmat Ullah:** funding acquisition, resources, validation, writing – review and editing. **Ehtasham Mustafa:** conceptualization, formal analysis, project administration, supervision, writing – review and editing. **Abdelfatah Ali:** conceptualization, formal analysis, project administration, supervision, validation, writing – review and editing.

Data Availability Statement

Data available on request from the authors. The data supporting the outcomes of this study are available based on the request from the corresponding author.

References

1. F. Alanazi, "Electric Vehicles: Benefits, Challenges, and Potential Solutions for Widespread Adaptation," *Applied Sciences* 13 (2023): 6016, [Internet]. 2023 May 13;13(10):6016. https://www.mdpi.com/2076-3417/13/10/6016/htm.

2. V. Boglou, C. S. Karavas, A. Karlis, K. G. Arvanitis, and I. Palaiologou, "An Optimal Distributed RES Sizing Strategy in Hybrid Low Voltage Networks Focused on EVs' Integration," *IEEE Access* 11 (2023): 16250–16270.

3. W. Pinthurat, B. Hredzak, G. Konstantinou, and J. Fletcher, "Techniques for Compensation of Unbalanced Conditions in LV Distribution Networks With Integrated Renewable Generation: An Overview," *Electric Power Systems Research* 214 (January 2023): 108932.

4. J. Bešić, A. Bosović, and M. Musić, "Analysis of the Impact of Unbalanced Connection of Consumers and Electric Vehicles on Voltage Variation and Voltage Unbalance," *B&H Electrical Engineering* 18, no. 1 (June 2024): 1–11.

5. S. Maji and P. Kayal, "A Simplified Multi-Objective Planning Approach for Allocation of Distributed PV Generators in Unbalanced Power Distribution Systems," *Renewable Energy Focus* 48 (March 2024): 100541.

6. A. M. Soliman, S. M. Emara, and M. N. F. Nashed, "Grid Performance Enhancement Study Under Restricted Placement and Sizing of PV Distributed Generation," *Journal of Electrical Engineering & Technology* 18, no. 1 (January 2023): 229–237, https://doi.org/10.1007/s42835-022-01219-8.

7. B. Mukhopadhyay and D. Das, "Multi-Objective Dynamic and Static Reconfiguration With Optimized Allocation of PV-DG and Battery Energy Storage System," *Renewable and Sustainable Energy Reviews* 124 (May 2020): 109777.

8. S. Alizadeh, M. Mahdavian, and E. Ganji, "Optimal Placement and Sizing of Photovoltaic Power Plants in Power Grid Considering Multi-Objective Optimization Using Evolutionary Algorithms," *Journal of Electrical Systems and Information Technology* 10:1 [Internet]. 10, no. 1 (January 2023): 7, https://doi.org/10.1186/s43067-023-00073-6.

9. N. Rehman, M. ud din Mufti, and N. Gupta, "Analytical Index-Based Allocation and Sizing of Lambert-W Modeled PV in An Active Distribution Network," *Energy Conversion and Management: X* 17 (January 2023): 100334.

10. A. M. Shaheen, R. A. El-Sehiemy, A. Ginidi, A. M. Elsayed, and S. F. Al-Gahtani, "Optimal Allocation of PV-STATCOM Devices in Distribution Systems for Energy Losses Minimization and Voltage Profile Improvement via Hunter-Prey-Based Algorithm," *Energies* 16, no. 6 (March 2023): 2790 [Internet], https://www.mdpi.com/1996-1073/16/6/2790/htm.

11. A. Selim, S. Kamel, A. A. Mohamed, and E. E. Elattar, "Optimal Allocation of Multiple Types of Distributed Generations in Radial Distribution Systems Using a Hybrid Technique," *Sustainability* 13, no. 12 (June 2021): 6644 [Internet], https://www.mdpi.com/2071-1050/13/12/6644/htm.

12. I. Khenissi, R. Sellami, M. A. Fakhfakh, and R. Neji, "Power Loss Minimization Using Optimal Placement and Sizing of Photovoltaic Distributed Generation Under Daily Load Consumption Profile With PSO and GA Algorithms," *Journal of Control, Automation and Electrical Systems* 32, no. 5 (October 2021): 1317–1331, https://doi.org/10.1007/s40313-021-00744-7.

13. T. T. Nguyen, T. T. Nguyen, and M. Q. Duong, "An Improved Equilibrium Optimizer for Optimal Placement of Photovoltaic Systems in Radial Distribution Power Networks," *Neural Computing and Applications* 34, no. 8 (April 2022): 6119–6148, https://doi.org/10.1007/s00521-021-06779-w.

14. M. Aref, V. Oboskalov, A. El-Shahat, and A. Y. Abdelaziz, "Modified Analytical Technique for Multi-Objective Optimal Placement of High-Level Renewable Energy Penetration Connected to Egyptian Power System," *Mathematics* 11, no. 4 (2023): 958 [Internet], https://www.mdpi.com/2227-7390/11/4/958/htm.

15. S. M. R. H. Shawon, X. Liang, and M. Janbakhsh, "Optimal Placement of Distributed Generation Units for Microgrid Planning in Distribution Networks," *IEEE Transactions on Industry Applications* 59, no. 3 (May 2023): 2785–2795.

16. A. Yadav, N. Kishor, and R. Negi, "Bus Voltage Violations under Different Solar Radiation Profiles and Load Changes With Optimally Placed and Sized PV Systems," *Energies* 16, no. 2 (January 2023): 653 [Internet], https://www.mdpi.com/1996-1073/16/2/653/htm.

17. T. Yuvaraj, K. R. Devabalaji, J. A. Kumar, S. B. Thanikanti, and N. I. Nwulu, "A Comprehensive Review and Analysis of the Allocation of Electric Vehicle Charging Stations in Distribution Networks," *IEEE Access* 12 (2024): 5404–5461.

18. A. Ali, H. H. H. Mousa, M. F. Shaaban, M. A. Azzouz, and A. S. A. Awad, "A Comprehensive Review on Charging Topologies and Power Electronic Converter Solutions for Electric Vehicles," *Journal of Modern Power Systems and Clean Energy* 12, no. 3 (May 2024): 675–694.

19. A. R. Singh, P. Vishnuram, S. Alagarsamy, et al., "Electric Vehicle Charging Technologies, Infrastructure Expansion, Grid Integration Strategies, and Their Role in Promoting Sustainable e-Mobility," *Alexandria Engineering Journal* 105 (October 2024): 300–330.

20. M. Bilal and M. Rizwan, "Intelligent Algorithm-Based Efficient Planning of Electric Vehicle Charging Station: A Case Study of Metropolitan City of India," *Scientia Iranica* 30, no. 2 (April 2023): 559–576, https://scientiairanica.sharif.edu/article_22425.html.

21. M. Nour, J. P. Chaves-Ávila, G. Magdy, and Á. Sánchez-Miralles, "Review of Positive and Negative Impacts of Electric Vehicles Charging on Electric Power Systems," *Energies* 13, no. 18 (September 2020): 4675 [Internet], https://www.mdpi.com/1996-1073/13/18/4675/htm.

22. P. Pradhan, I. Ahmad, D. Habibi, G. Kothapalli, and M. A. S. Masoum, "Reducing the Impacts of Electric Vehicle Charging on Power Distribution Transformers," *IEEE Access* 8 (2020): 210183–210193.

23. Y. Zhang, Q. Zhang, A. Farnoosh, S. Chen, and Y. Li, "GIS-Based Multi-Objective Particle Swarm Optimization of Charging Stations for Electric Vehicles," *Energy* 169 (February 2019): 844–853.

24. A. Pal, A. Bhattacharya, and A. K. Chakraborty, "Allocation of Electric Vehicle Charging Station Considering Uncertainties," *Sustainable Energy, Grids and Networks* 25 (March 2021): 100422.

25. M. Bilal and M. Rizwan, "Integration of Electric Vehicle Charging Stations and Capacitors in Distribution Systems With Vehicle-To-Grid Facility," *Energy Sources, Part A: Recovery, Utilization, and Environmental Effects* 47, no. 1 (December 2025): 7700–7729, https://doi.org/10.1080/15567036.2021.1923870.

26. S. Sheik Mohammed, F. Titus, S. B. Thanikanti, S. M. Sulaiman, S. Deb, and N. M. Kumar, "Scheduling Optimization of Plug-In Electric Vehicle in a PV Powered Grid-Connected Charging Station Based on Day-Ahead Solar Energy Forecasting in Australia," *Sustainability* 14, no. 6 (March 2022): 3498 [Internet], https://www.mdpi.com/2071-1050/14/6/3498/htm.

27. H. Martin, R. Buffat, D. Bucher, J. Hamper, and M. Raubal, "Using Rooftop Photovoltaic Generation to Cover Individual Electric Vehicle Demand—A Detailed Case Study," *Renewable and Sustainable Energy Reviews* 157 (April 2022): 111969.

28. D. Srinivas and D. M. R. Reddy, "Optimal Location of Electric Vehicle Charging Station in Reconfigured Radial Distribution Network," *International Journal of Electrical and Electronics Research* 11, no. 4 (October 2023): 1065–1071.

29. R. J. Venkatesh, R. Priya, P. Hemachandu, and C. V. K. Reddy, "An Optimization Approach Control of EV Solar Charging System With

Step-Up DC–DC Converter," *Analog Integrated Circuits and Signal Processing* 119, no. 2 (May 2024): 215–232, https://doi.org/10.1007/s10470-024-02253-4.

30. W. S. Tounsi Fokui, M. J. Saulo, and L. Ngoo, "Optimal Placement of Electric Vehicle Charging Stations in a Distribution Network With Randomly Distributed Rooftop Photovoltaic Systems," *IEEE Access* 9 (2021): 132397–132411, https://ieeexplore.ieee.org/document/9537756.

31. E. A. Rene, W. S. Tounsi Fokui, and P. K. Nembou Kouonchie, "Optimal Allocation of Plug-In Electric Vehicle Charging Stations in the Distribution Network With Distributed Generation," *Green Energy and Intelligent Transportation* 2, no. 3 (June 2023): 100094.

32. A. R. A. Alphonse, A. P. P. G. Raj, and M. Arumugam, "Simultaneously Allocating Electric Vehicle Charging Stations (EVCS) and Photovoltaic (PV) Energy Resources in Smart Grid Considering Uncertainties: A Hybrid Technique," *International Journal of Energy Research* 46, no. 11 (September 2022): 14855–14876.

33. M. Z. Zeb, K. Imran, A. Khattak, et al., "Optimal Placement of Electric Vehicle Charging Stations in the Active Distribution Network," *IEEE Access* 8 (2020): 68124–68134.

34. A. Asaad, A. Ali, K. Mahmoud, et al., "Multi-Objective Optimal Planning of EV Charging Stations and Renewable Energy Resources for Smart Microgrids," *Energy Science & Engineering* 11, no. 3 (March 2023): 1202–1218.

35. V. K. B. Ponnam and K. Swarnasri, "Multi-Objective Optimal Allocation of Electric Vehicle Charging Stations and Distributed Generators in Radial Distribution Systems Using Metaheuristic Optimization Algorithms," *Engineering, Technology & Applied Science Research [Internet]* 10, no. 3 (June 2020): 5837–5844, https://www.etasr.com/index.php/ETASR/article/view/3517.

36. M. J. H. Moghaddam, A. Kalam, J. Shi, S. A. Nowdeh, F. H. Gandoman, and A. Ahmadi, "A New Model for Reconfiguration and Distributed Generation Allocation in Distribution Network Considering Power Quality Indices and Network Losses," *IEEE Systems Journal* 14, no. 3 (September 2020): 3530–3538.

37. A. Ali, D. Raisz, K. Mahmoud, and M. Lehtonen, "Optimal Placement and Sizing of Uncertain PVs Considering Stochastic Nature of PEVs," *IEEE Transactions on Sustainable Energy* 11, no. 3 (July 2020): 1647–1656.

38. M. Bilal, M. Rizwan, I. Alsaidan, and F. M. Almasoudi, "AI-Based Approach for Optimal Placement of EVCS and DG With Reliability Analysis," *IEEE Access* 9 (2021): 154204–154224.

39. F. Ahmad and M. Bilal, "Allocation of Plug-In Electric Vehicle Charging Station With Integrated Solar Powered Distributed Generation Using an Adaptive Particle Swarm Optimization," *Electrical Engineering* 106, no. 3 (June 2024): 2595–2608, https://doi.org/10.1007/s00202-023-02087-9.

40. S. Mondal and M. De, "Optimal Allocation and Smart Scheduling of Distributed Energy Resources and Electrical Vehicles to Enhance Economical Operation of Unbalanced Distribution System," *Electrical Engineering* 105, no. 6 (December 2023): 3493–3510.

41. N. K. K. Sabhahit and J. N. Jadoun VK. Voltage Unbalance Assessment in a Distribution System Incorporated with Renewable-Based Sources and Electric Vehicles in an Uncertain Environment. IET Renewable Power Generation [Internet]. 2024 [cited 2024 Sep 3]; https://doi.org/10.1049/rpg2.13009.

42. S. Mondal and M. De, *Wild Horse Optimizer Based Optimal Allocation of DG and Capacitor Bank for Unbalanced Distribution System in Presence of Plugged-in EV* (GlobConET 2022: IEEE IAS Global Conference on Emerging Technologies, 2022). 2022, 423–428.

43. S. Toghranegar, A. Rabiee, and S. M. Mohseni-Bonab, "Increasing Unbalanced Distribution Network's Hosting Capacity for Distributed Energy Resources by Voltage Regulators," *IEEE Access* 11 (2023): 22664–22679.

44. A. Almazroui and S. Mohagheghi, "Coordinated Control of Electric Vehicles and PV Resources in an Unbalanced Power Distribution System," *Energies* 15, no. 24 (December 2022): 9324 [Internet], https://www.mdpi.com/1996-1073/15/24/9324/htm.

45. W. Alabri and D. Jayaweera, "Voltage Regulation in Unbalanced Power Distribution Systems With Residential PV Systems," *International Journal of Electrical Power & Energy Systems* 131 (October 2021): 107036.

46. T. Antić, T. Capuder, and M. Bolfek, "A Comprehensive Analysis of the Voltage Unbalance Factor in PV and EV Rich Non-Synthetic Low Voltage Distribution Networks," *Energies* 14, no. 1 (2021): 117 [Internet], https://www.mdpi.com/1996-1073/14/1/117/htm.

47. L. F. Silveira, M. S. Martins, L. Kräulich, et al., "A New Approach for Mitigating Voltage Unbalance in a Three-Phase Two-Wire Rural Distribution Network," *Electric Power Systems Research [Internet]* 237 (December 2024): 111042, https://www.sciencedirect.com/science/article/abs/pii/S0378779624009283.

48. M. Jalili, M. Sedighizadeh, and A. Sheikhi Fini, "Optimal Operation of the Coastal Energy Hub Considering Seawater Desalination and Compressed Air Energy Storage System," *Thermal Science and Engineering Progress* 25 (October 2021): 101020.

49. X. Lu, K. Zhou, S. Yang, and H. Liu, "Multi-Objective Optimal Load Dispatch of Microgrid With Stochastic Access of Electric Vehicles," *Journal of Cleaner Production* 195 (September 2018): 187–199.

50. M. Mohiti, H. Monsef, and H. Lesani, "A Decentralized Robust Model for Coordinated Operation of Smart Distribution Network and Electric Vehicle Aggregators," *International Journal of Electrical Power & Energy Systems* 104 (January 2019): 853–867.

51. A. Ali, K. Mahmoud, and M. Lehtonen, "Optimization of Photovoltaic and Wind Generation Systems for Autonomous Microgrids With PEV-Parking Lots," *IEEE Systems Journal* 16, no. 2 (June 2022): 3260–3271.

52. G. Abdulnasser, A. Ali, M. F. Shaaban, and E. E. M. Mohamed, "Optimizing the Operation and Coordination of Multi-Carrier Energy Systems in Smart Microgrids Using a Stochastic Approach," *IEEE Access* 11 (2023): 58470–58490.

53. S. Mirjalili, S. M. Mirjalili, and A. Lewis, "Grey Wolf Optimizer," *Advances in Engineering Software [Internet]* 69 (March 2014): 46–61, https://www.sciencedirect.com/science/article/abs/pii/S0965997813001853.

54. OpenDSS download | SourceForge.net [Internet]. [cited 2024 Sep 3], https://sourceforge.net/projects/electricdss/.

55. Y. Bot, B. Naama, A. Yousfi, A. Allali, and M. Denai, "Control of Line Voltage Unbalance Factor in Three-Phase Distribution Grids Caused by Single-Phase Photovoltaic Systems," *Journal of Renewable and Sustainable Energy [Internet]* 14, no. 2 (2022): 026301.

56. L. Le Dinh, D. Vo Ngoc, and P. Vasant, "Artificial Bee Colony Algorithm for Solving Optimal Power Flow Problem," *The Scientific World Journal* 2013, no. 1 (2013 Jan 1): 159040, https://doi.org/10.1155/2013/159040.

57. Y. Hou, H. Gao, Z. Wang, C. Du, et al., "Improved Grey Wolf Optimization Algorithm and Application," *Sensors* 22, no. 10 (May 2022): 3810 [Internet], https://www.mdpi.com/1424-8220/22/10/3810/htm.